*Pharmaceutical Research, Vol. 25, No. 1, January 2008 (© 2007)*
DOI: 10.1007/s11095-007-9456-4

*Research Paper*

# Microenvironment-Controlled Encapsulation (MiCE) Process: Effects of PLGA Concentration, Flow Rate, and Collection Method on Microcapsule Size and Morphology

**Connie Snider,[1] Sang-Youp Lee,[2,3] Yoon Yeo,[1] Gérald J. Grégori,[2,3] J. Paul Robinson,[2,3] and Kinam Park[1,4,5]**

*Received April 29, 2007; accepted September 6, 2007; published online October 4, 2007*

***Purpose.*** To evaluate the real-time effects of formulation and instrumental variables on microcapsule formation via natural jet segmentation, a new microencapsulation system termed the microenvironment-controlled encapsulation (MiCE) process was developed.
***Methods.*** A modified flow cytometer nozzle hydrodynamically focuses an inner drug and outer polymer solution emanating from a coaxial needle assembly into a two-layer compound jet. Poly(lactic-*co*-glycolic acid) (PLGA) dissolved in a water-miscible organic solvent resulted in formation of reservoir-type microcapsules by interfacial phase separation induced at the boundary between the PLGA solution and aqueous sheath.
***Results.*** The MiCE process produced microcapsules with mean diameters ranging from 15–25 μm. The resultant microcapsule size distribution and number of drug cores existing within each microcapsule was largely influenced by the PLGA concentration and microcapsule collection method. Higher PLGA concentrations yielded higher mean diameters of single-core microcapsules. Higher drug solution flow rates increased the core size, while higher PLGA solution flow rates increased the PLGA film thickness.
***Conclusion.*** The MiCE microencapsulation process allows effective monitoring and control of the instrumental parameters affecting microcapsule production. However, the microcapsule collection method in this process needs to be further optimized to obtain microcapsules with desired morphologies, precise membrane thicknesses, high encapsulation efficiencies, and tight size distributions.

**KEY WORDS:** flow cytometry; interfacial phase separation; microcapsules; PLGA; Rayleigh breakup.

## INTRODUCTION

Controlled release drug delivery systems have been frequently employed to maximize the therapeutic efficacy of numerous active pharmaceutical ingredients. Microencapsulation is a technique that can bring about *in vivo* controlled drug release through formation of a rate-controlling biodegradable polymer matrix around the drug contents. By parenterally administering microencapsulated therapeutics, patients can maintain adequate blood levels of active for weeks or even months, thereby diminishing patient discomfort and increasing compliance (1–4). One of the most common biodegradable polymers employed in microencapsulation is poly(lactic-*co*-glycolic acid) (PLGA). This polymer matrix also serves a barrier, which can protect fragile protein drugs from *in vivo* enzymatic degradation and thus significantly lengthen their very short half-lives (5–8). Because proteins can be denatured at the solid/liquid (9) and water/organic solvent (10) interfaces, the optimal microcapsule morphology for protein drug delivery is a single drug core, i.e., reservoir-type microcapsule, since this exposes the protein to the least PLGA surface area.

To achieve the best control over microcapsule size and morphology, a new production process was designed utilizing a natural drop formation mechanism. In this process, the droplets are created via jet breakup due to instabilities in the Rayleigh breakup regime, which overcome the stabilizing surface tension forces of the jet. Under laminar flow conditions, single inviscid liquid jets in this regime become unstable due to axisymmetric disturbances when the disturbance wavelength is longer than the jet circumference (11,12). Numerous instruments employ Rayleigh jet instability theories to produce small and homogeneous droplets. One representative example is a flow cytometer, an instrument widely used to separate, analyze, and sort biological cells and other particles (13,14). In flow cytometry, an aqueous sample solution jet containing single cells is coaxially accelerated and narrowed by a surrounding aqueous buffer solution (i.e., sheath). This process is known as hydrodynamic focusing and

[1] Department of Pharmaceutics, Purdue University, West Lafayette, Indiana 47907, USA.
[2] Department of Basic Medical Sciences, Purdue University, West Lafayette, Indiana 47907, USA.
[3] Department of Purdue Cytometry Laboratories, Purdue University, West Lafayette, Indiana 47907, USA.
[4] Department of Biomedical Engineering, Purdue University, BMED Building, 206 S. Martin Jischke Drive, West Lafayette, Indiana 47907, USA.
[5] To whom correspondence should be addressed. (e-mail: kpark@purdue.edu)

is brought about by an orifice at the tip of the flow cytometer nozzle (flow chamber), which causes significant cross-sectional area change. Upon exit from the orifice, the coaxially-aligned jet (i.e., compound jet) undergoes breakup via Rayleigh-type instability. The compound jet is typically referred to as a coaxially-aligned jet consisting of two or more immiscible fluids. Hertz and Hermanrud *et al.* (15) investigated the two-layered compound jet instability experimentally. In this study, they showed that compound jet breakup due to capillary instability can be identical to the single jet under conditions which allow the compound jet to behave like a single jet. This single jet condition can be attained by adjusting the jet diameter and/or fluid properties.

Several groups have demonstrated the application of compound jet breakup in microencapsulation. An exemplary device used to create microspheres and microcapsules has been designed by Berkland *et al.* (16–18) Their system utilizes a coaxial nozzle, which delivers inner and outer solutions, all surrounded by an aqueous sheath. The formed double-layer jet is immediately broken up by ultrasonic excitation and then carried into the collection bath by the annular carrier stream in air. Loscertales *et al.* (19) introduced a flow focusing encapsulation method in which a two-layer compound jet breaks up in air under electro-hydrodynamic forces. One disadvantage of this technology is that the fluids need to be conductive. Gañán-Calvo *et al.* (20) generated mono-dispersed air bubbles on the micron scale using capillary flow focusing. More rapid breakup of the air stream within the liquid jet was observed when a large property difference existed between the two fluids. This system is similar to the conventional flow cytometer with a jet-in-air type flow chamber, with the exception being that the capillary delivers air instead of sample solution. Utada *et al.* (21) developed a microdevice for controlled double emulsion generation utilizing a large viscosity difference between the sheath and jetting fluids. Higher viscosity sheath fluids exert viscous stress on the compound jet, inducing jet breakup. To force the compound jet to behave like a jet composed of only one component, resulting in jet breakup synchronization, viscosities of the jetting fluids need to be matched. Jet breakup synchronization is necessary in microencapsulation since it can best ensure that each polymer solution droplet contains one drug core. Therefore, the difficulties in compound jet breakup for single-core microcapsule formation lie in matching the breakup timing of the each compound jet component because the wavelength response related to the perturbation is a function of the fluid properties (22) and jet diameter (23).

We have explored a new microencapsulation method based on conventional flow cytometry, termed the microenvironment-controlled encapsulation (MiCE) process. The system was designed to fragment the bulk liquid into the desired volumes without a stressful emulsification step. In the MiCE process, a two-layer compound jet formed via hydrodynamic focusing under laminar flow conditions breaks up into compound droplets due to jet instabilities within a co-flowing aqueous sheath. On our system, the microencapsulation process can be viewed in real-time, allowing us to evaluate the effects of formulation and instrumental parameters on jet breakup. In the current study, we first discuss properties such as the viscosity and density of each working fluid, which were experimentally determined. Second, the effects of PLGA solution viscosity on the microcapsule diameters and morphology, as well as the effects of working solution flow rate on microcapsule size, are investigated. In addition, the challenges encountered during microcapsule collection, due to the high shear forces generated in the bath, are discussed. The scope of this study was limited to examining formulation and instrumental parameters on jet breakup into individual droplets and subsequent collection in the collection bath.

## Principles of the MiCE Process

The MiCE system was built upon conventional flow cytometry technology, but installed on an optical table within a chemical hood in order to minimize vibrations and isolate solvent fumes. Major modifications were made to the sample insertion needle and flow chamber. Fig. 1A displays a schematic diagram of the MiCE system. Unlike the single needle sample introduction on a conventional flow cytometer, the drug and polymer solutions were fed through a coaxial needle assembly on this system. An aqueous core solution, containing lysozyme, a model protein, in distilled water, was fed through the center needle of the coaxial needle assembly, while PLGA in ethyl acetate was fed through the outer needle. Inner and outer stainless capillary needles were coaxially aligned using a corrugated outer needle, and separate liquid flows into each needle were attained by connecting inner and outer needles with a high pressure polyetheretherketone tee. The dimensions of the capillary needles were 1/32 in (OD)/0.025 in (ID) for the inner needle and 1/16 in (OD)/0.0525 in (ID) for the outer needle. Distilled water was employed as the sheath fluid and was inputted through a side port in the flow chamber. The three working fluids, aqueous drug solution, polymer solution, and aqueous sheath fluid, were accelerated together into a quartz microchannel attached to the tip of the flow chamber (Fig. 1B), forming a hydrodynamic flow focusing region. This region is where the transformation from macroscale into microscale flow occurs and, consequently, enables the disintegration into desired small volumes.

The perturbation begins on the compound jet surface and after the compound jet grows sufficiently, disintegration occurs under the dominating instability within the co-flowing sheath fluid in the microchannel. The dimensions of the microchannel were 250 μm×250 μm×10.3 mm, which simplifies the compound jet breakup process since the co-flowing sheath fluid is bounded by the microchannel and thus, eliminates surface perturbations induced by another medium, such as air. Because a water miscible solvent (i.e. ethyl acetate) comprises the polymer solution, most of it diffuses into the surrounding sheath fluid, resulting in polymer precipitation. This process is known as interfacial phase separation (24) and exposes the protein drug to minimal chemical stress, especially when reservoir-type microcapsules are formed.

The hydrodynamic focusing region in the flow chamber, jet breakup, and subsequent microcapsule formation were monitored with a 12-bit monochrome CCD camera and a stroboscopic illumination system comprised of an LED strobe light (Luxeon III Star; Philips Lumileds Lighting; San Jose, CA). The CCD camera and strobe light were synchronously operated using a digital delay pulse generator (565; Berkeley Nucleonics Corp.; San Rafael, CA). The

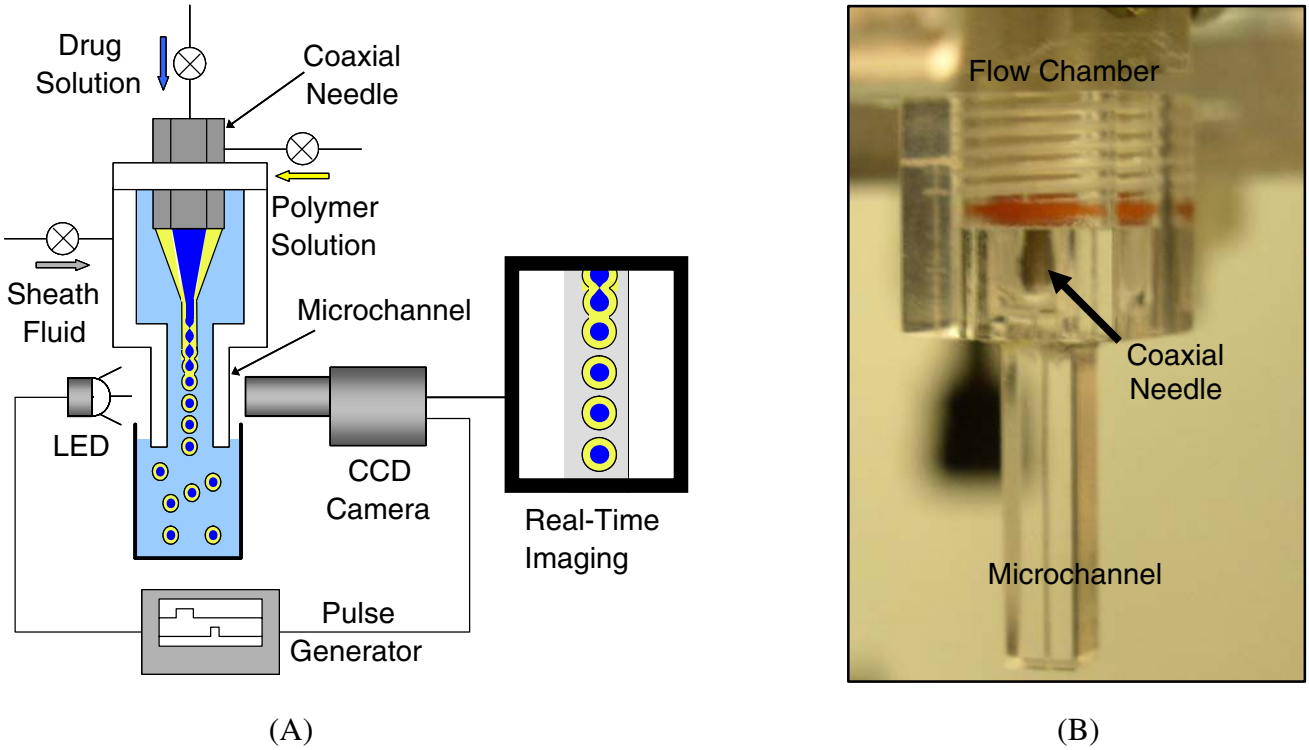


**Fig. 1.** **A** Schematic diagram of the MiCE system (not to scale). **B** Photo of the flow chamber with a square microchannel.

average speed of the stream was about 3.5 m/s, and in order to capture a still image of microcapsule generation, the light source was operated with a very short pulse of 0.1–1.0 μs during the camera exposure time of 10 μs. This imaging also allows one to determine whether the jets and subsequent breakup are stable, in addition to the morphology and structural integrity of the formed microcapsules within the sheath jet. To carry out this imaging, a special flow chamber design was needed, one that could allow us to view inside the flow chamber and microchannel through a flat and transparent medium, thereby avoiding distortion. Therefore, the flow chamber was custom-built in a cubic rather than conical form with transparent acrylic, while the microchannel was also created in cubic form and comprised of transparent quartz.

All working solutions were driven into the system by pressurizing the fluid containers with air, and their flow rates were precisely controlled with digital pressure valves (VSO-EP; Parker Hannifin Corp.; Cleveland, OH). The flow rate of the sheath fluid was measured with a rotameter, while the flow rates of the polymer solution and core fluid were measured using weighing balances. The Reynolds number based on the sheath flow rate was around 1100, placing the flow in the laminar regime. Fig. 2 shows the hydrodynamic focusing region at different flow rate combinations. Inside the flow chamber, all flows were stable, and thus the shape of the coaxial stream depended only on the fluid properties and driving pressures. Because the flow rates greatly affect the membrane thickness and core sizes then, these two parameters were optimized during each sample run via real-time imaging to ensure a proper pressure balance between the two adjacent component fluids for desired microcapsule formation. As was previously mentioned, microcapsule formation

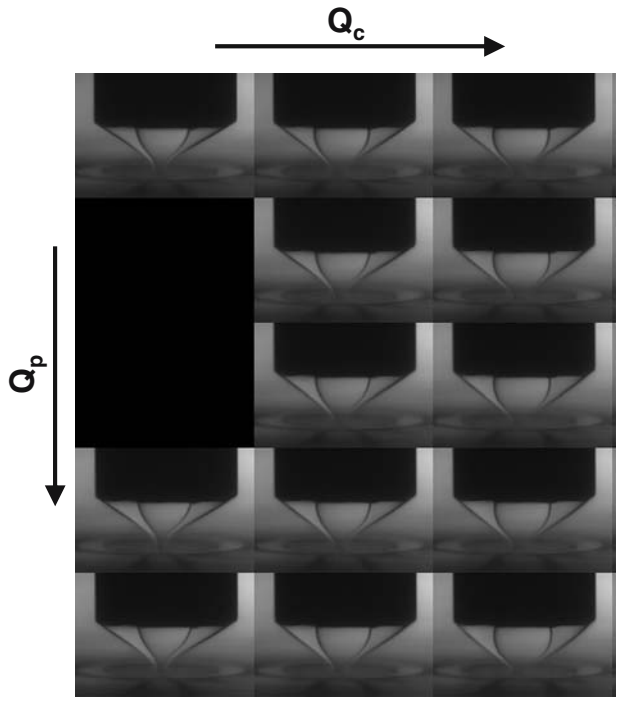


**Fig. 2.** Images of the hydrodynamic focusing region within the flow chamber showing the effect of core and polymer solution flow rates on the core size and PLGA membrane thickness. Aqueous core fluid: distilled water.

takes place via the growth of instabilities along the jet surface. When the wavelength of these instabilities exceeds some critical value, droplet formation takes place, followed by interfacial phase separation. However, to form the desired reservoir-type microcapsules, the breakup of both the aqueous core and polymer solutions needs to be synchronized. This was done by precisely controlling the air pressures that drive each component liquid through the system using the digital pressure valves, while concurrently observing the jet breakup dynamics in the flow chamber.

## MATERIALS AND METHODS

### Materials

Poly(D,L-lactide-*co*-glycolide) (PLGA) (#50DG065; lactide/glycolide ratio=50:50, intrinsic viscosity=0.58 dL/g, MW≈80 kDa) was purchased from Birmingham Polymers (Birmingham, AL). Lysozyme (#L6876) and Nile Red (#N3013) were purchased from Sigma (St. Louis, MO). Poly(vinyl alcohol) (98.0–98.8 mol% hydrolyzed, MW= 195 kDa; #10851) was purchased from Fluka (Milwaukee, WI). Ethyl acetate (ethyl acetate) (#4992) was purchased from Mallinckrodt Chemicals (Hazelwood, MO). The bicinchoninic acid protein assay kit (#23225) was obtained from Pierce (Rockford, IL).

### Fluid Property Measurements

#### *Viscosity*

The rheological characteristics of various concentrations of lysozyme in distilled water and PLGA in ethyl acetate were measured using a viscometer (DV-II+ Pro; Brookfield Engineering; Middleboro, MA) equipped with a temperature-controlled circulating bath (Polystat; Cole-Parmer; Vernon Hills, IL). Five measurements were taken for each sample at a shear rate of 33.00 $s^{-1}$. To determine the accuracy of our viscosity measurements, the viscosities of pure distilled water and ethyl acetate were measured and found to be in good agreement with published values (25).

#### *Density*

To measure the densities of various PLGA and lysozyme solutions at room temperature (~25°C), 1 and 5 mL glass volumetric flasks were first weighed on an analytical balance (AB104-S; Mettler Toledo; Columbus, OH), filled up to the line with solution, and weighed again. The solution weight divided by the flask volume gave the density. 1, 2, 3, and 5% PLGA in EA solutions were measured, along with 1, 2, and 3% lysozyme.

### Flow Rate Determination

To obtain the mass of the aqueous core and polymer solutions used during each sample run, the pressurized bottles containing each solution were weighed on two separate macrobalances (L2200S; Sartorius Corp; Edgewood, NY) (B502-S; Mettler Toledo; Columbus, OH). The time of each sample run was measured with a stopwatch, yielding the solution flow rates.

### Microcapsule Preparation

An aqueous core solution, containing lysozyme in distilled water, was fed through the center needle of the coaxial needle assembly (Fig. 1B), while PLGA in ethyl acetate was fed through the outer needle. A distilled water sheath was fed directly into the flow chamber at a flow rate significantly higher than either core solution, which led to the hydrodynamic focusing of the inner two-layered compound jet. All working solutions were fed into the system via compressed air, and their flow rates were precisely controlled by digital pressure valves (VSO-EP; Parker Hannifin Corp.; Cleveland, OH). The final three-layer compound jet then entered the quartz microchannel (diameter=250 μm) (Fig. 1B). Microcapsules were collected by submerging the microchannel tip in a 3.5 mL quartz cuvette placed on a stainless steel stand. The stand and cuvette were placed in an empty 400 mL glass collection vessel, which collected overflow from the cuvette.

After microcapsule collection, the collection vessel contents were magnetically stirred for 30 min and then allowed to sit for 1.5 h, to allow for solvent evaporation and microparticle settling. Most of the supernatant was then poured off, and the remaining contents were saved for analysis without washing, to prevent microcapsule rupturing. A portion of the microcapsules were refrigerated for particle size analysis and bright field imaging, while the remaining portion was frozen and then lyophilized (Flexi-Dry MP; FTS Systems; Stone Ridge, NY) for about 48 h.

### Microscopic Imaging

#### *Bright Field Microscopy*

The microcapsule morphology and size was observed using bright field microscopy (Labophot-2; Nikon USA; Mellville, NY). Samples were first placed on a glass microscope slide with a glass cover slip and then imaged with an 8-bit monochrome CCD camera (JE2362; Javelin Electronics; Los Angeles, CA).

#### *Fluorescence Microscopy*

The profile of microcapsules were observed using an upright fluorescence microscope (BX51; Olympus America; Mellville, NY) equipped with a 12-bit monochrome CCD camera (Retiga 2000R; QImaging Corp.; Burnaby, BC, Canada) with an RGB filter and a 100 W mercury lamp. The polymer membrane was stained with Nile Red fluorescent dye. A few drops of the microcapsule-containing collection bath were withdrawn, placed on a glass microscope slide, and covered with a glass cover slip.

#### *Scanning Electron Microscopy*

The freeze-dried microcapsule size and morphology were characterized using scanning electron microscopy

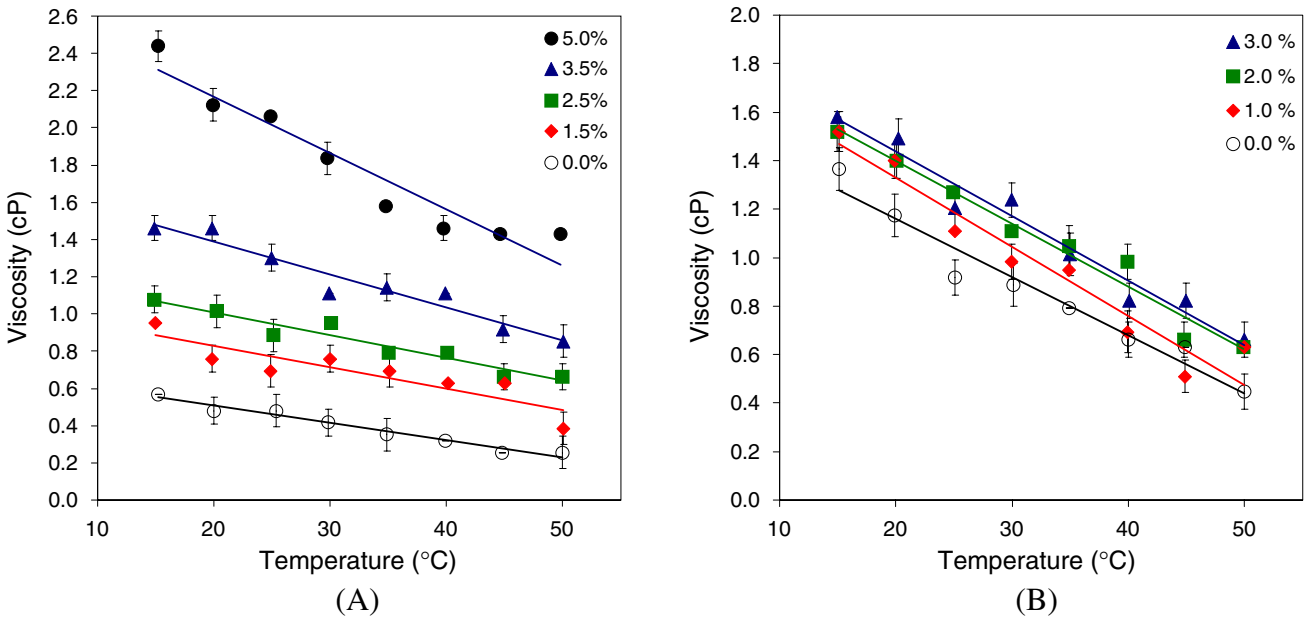


**Fig. 3.** Viscosities of **A** PLGA in ethyl acetate and **B** lysozyme in distilled water with respect to temperature. Viscosities of PLGA and lysozyme solutions were measured at concentrations of 0.0, 1.5, 2.5, 3.5, and 5.0%, and 0.0, 1.0, 2.0, and 3.0%, respectively. (0.0% in both **A** and **B** indicates pure solvent).

(JEOL JSM-840; JEOL USA; Peabody, MA). The samples were first affixed to aluminum specimen stubs using double-sided adhesive tape and then coated with gold-palladium in argon gas using a sputter coater (Hummer I; Anatech Ltd.; Hayward, CA). The coated microcapsules were then observed and imaged using SEM with an accelerating voltage of 4 kV, a 70 μm objective aperture, a working distance of 15 mm, and a probe current of $3\times10^{-11}$ A.

### Particle Size Analysis

The mean diameters of the microcapsules were acquired in the wet state (i.e. distilled water collection bath) using a particle size analyzer (S3500; Microtrac; Montgomeryville, PA) and the volume distribution. (For Batch #1, $N$=1, while for Batch #2–4, $N$=3.) Prior to analysis, any debris or ruptured microcapsules were removed from the wet sample by filtering through an

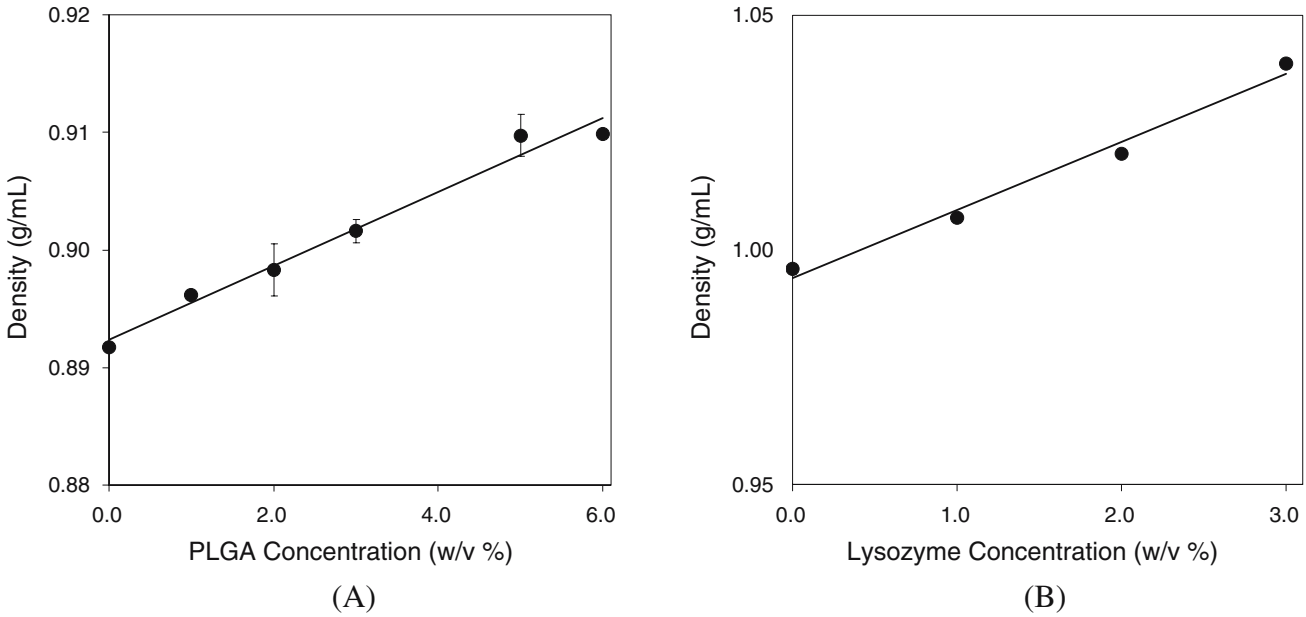


**Fig. 4.** Densities of **A** PLGA in ethyl acetate and **B** lysozyme in distilled water at various concentrations. (0.0% in both **A** and **B** indicates pure solvent).

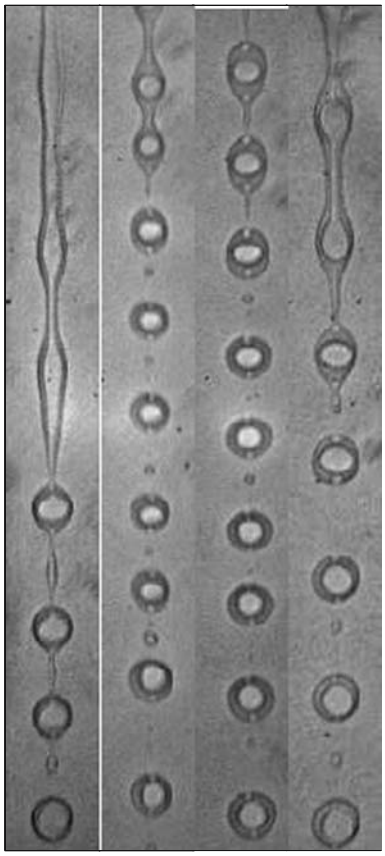


**Fig. 5.** Microcapsule generation within the square microchannel using **A** 5% PLGA solution and a low–high–medium (L–H–M) viscosity combination of sheath, PLGA solution, and lysozyme solution, **B** 3.5% PLGA solution (L–H–H), **C** 2.5% PLGA solution (M–L–H), and **D** 1.5% PLGA solution (M–L–H). $Q_{jet}/Q_{sheath}$ was **A** 0.022, **B** 0.014, **C** 0.025, and **D** 0.025, respectively.

ASTM E-11 test sieve (#0310023; Newark Wire Cloth Co.; Clifton, NJ) with an opening size of 106 μm (US Standard #140).

## RESULTS AND DISCUSSION

### Physical Properties of PLGA and Lysozyme Solutions

The jet breakup process greatly depends on fluidic properties such as density, viscosity, and interfacial tension. The rheological properties, viscosity and density, of PLGA and lysozyme solutions were measured at various concentrations. Properties of fluids comprising the compound jet play important roles as design parameters because microcapsule morphology and size are a function of these properties. The pure solvents for each solution, i.e. distilled water and ethyl acetate, were also measured and then compared to published values (25) in order to validate the current measurements. The mean viscosity for distilled water at 25°C was 0.918 cP, which is slightly larger than the published value of 0.890 cP, while the mean viscosity for pure ethyl acetate was 0.480 cP at 25°C, which is in close agreement with the published value of 0.423 cP.

Fig. 3A and B show the temperature-dependent dynamic viscosities of PLGA and lysozyme solutions, respectively, at various concentrations. The viscosities of all the tested solutions decreased with increasing temperature and for lowered solute concentrations. The viscosity of lysozyme solution decreased almost in parallel with pure water as the temperature increased (Fig. 3B), while the viscosity of PLGA solution exhibited steeper decreases with temperature at greater solute concentration (Fig. 3A). Thus, at lower temperatures, PLGA solution displays more distinctive viscosity changes with concentration. For example, at 25°C, the viscosity of 3% lysozyme solution was about 1.3 cP, and the viscosities of 5, 3.5, 2.5, and 1.5% PLGA solutions were about 2.1, 1.4, 1.0, and 0.8 cP, respectively. Thus, the relative viscosities between 5, 3.5, 2.5, and 1.5% PLGA solution and lysozyme solution ($\mu_{PLGA}/\mu_{lysozyme}$) are about 1.6, 1.1, 0.8, and 0.6, respectively, and between 5, 3.5, 2.5, and 1.5% PLGA solution and water sheath ($\mu_{PLGA}/\mu_{sheath}$) are about 2.3, 1.6, 1.1, and 0.9, respectively.

Density changes for various solute concentrations were not as drastic as the viscosity changes. Fig. 4 shows these density variations at 25°C. Compared to the relative viscosities, the relative densities between the two adjacent fluids were indistinctive. $\rho_{PLGA}/\rho_{lysozyme}$ was 0.875, 0.867, 0.864, and 0.862, and $\rho_{PLGA}/\rho_{sheath}$ was 0.913, 0.905, 0.902, and 0.900 for 5, 3.5, 2.5, and 1.5% PLGA in ethyl acetate, respectively. Thus, PLGA solutions at concentrations less than or equal to 5% were always lighter than lysozyme solution and sheath fluid. Since the interfacial tension between PLGA solution and distilled water was not determined, the interfacial tension value for ethyl acetate and distilled water was employed for analysis (26).

### Microcapsule Generation

Fig. 5 shows successful microcapsule generation in the square microchannel at four different PLGA concentrations: 5,

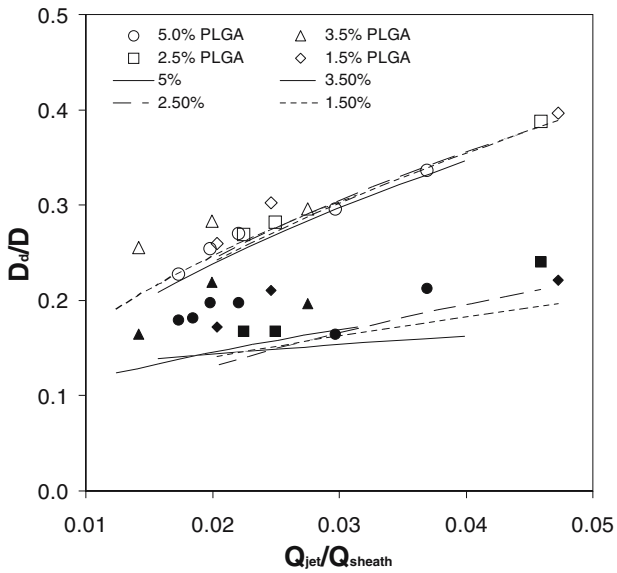


**Fig. 6.** Microcapsule and core diameters in the microchannel. The *open symbols* indicate microcapsule diameter, while the *solid symbols* indicate core diameter. The analytical results are shown with different *lines*.

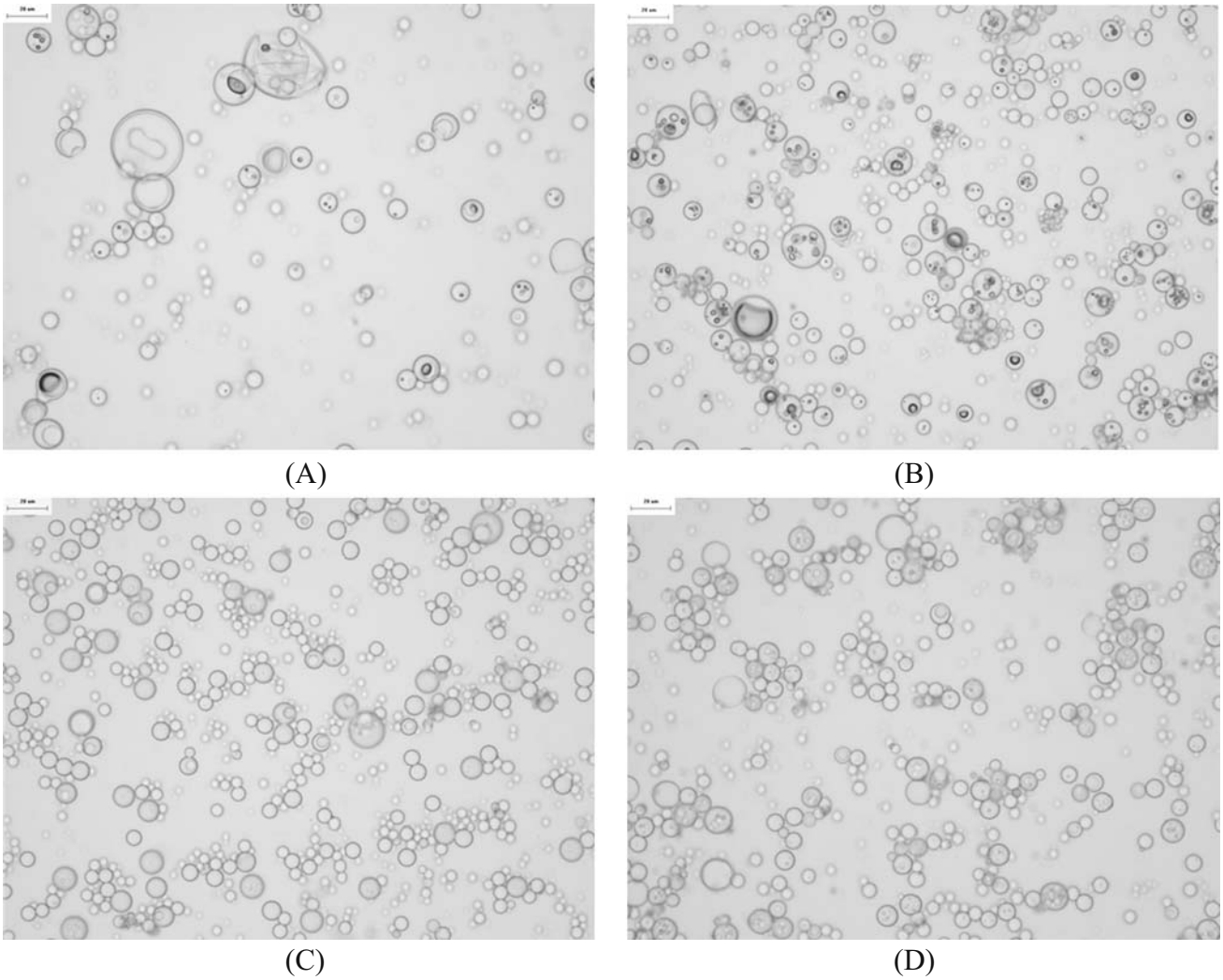


**Fig. 7.** Bright field images of microcapsules produced using the MiCE process and **A** 5% PLGA in ethyl acetate, **B** 3.5% PLGA in ethyl acetate, **C** 2.5% PLGA in ethyl acetate, and **D** 1.5% PLGA in ethyl acetate. Aqueous core solution: 3% lysozyme in distilled water. Sheath and bath: distilled water. *Scale bars*=20 μm.

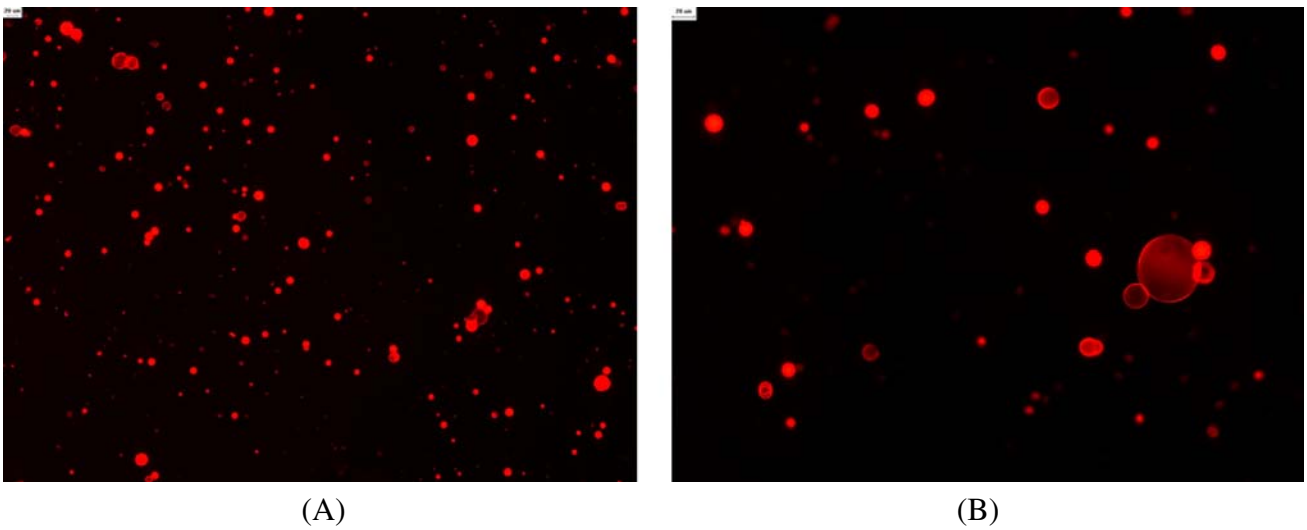


**Fig. 8.** Fluorescent images of microcapsules produced using the MiCE process. Aqueous core solution: 3% lysozyme in distilled water. Polymer solution: 5% PLGA in EA with 0.0014% Nile Red. Sheath: distilled water. Bath: 0.5% PVA (MW=195 kDa) in distilled water. *Scale bars*=20 μm.

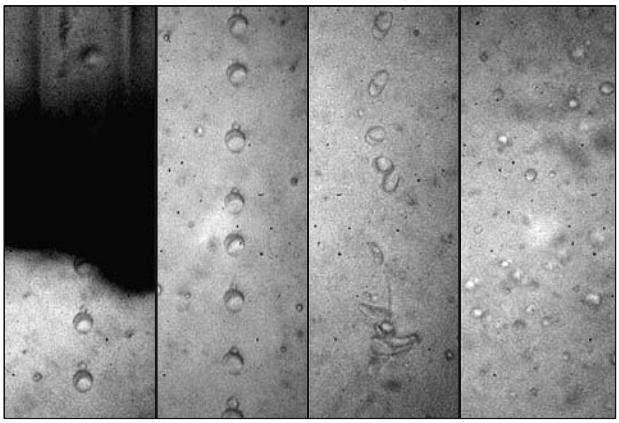


**Fig. 9.** Microcapsules in the distilled water collection bath. **A** Microcapsules exiting the microchannel. **B** Stable microcapsule formation in the initial portion of the collection bath. **C** Microcapsules subjected to significant shear forces from the stagnant collection bath. **D** Microcapsules undergoing secondary breakup.

3.5, 2.5, and 1.5% PLGA in ethyl acetate. The microcapsules appear to be evenly spaced with satellite droplets in between them within the microchannel. At 25°C, the viscosities of 5, 3.5, 2.5, and 1.5% PLGA solutions were about 2.1, 1.3, 0.9, and 0.8 cP, while a 3% lysozyme solution had an approximate viscosity of 1.3 cP. Therefore, the viscosity combinations of sheath, PLGA solution, and lysozyme solution were low–high–medium (L–H–M) for Fig. 5A, L–H–H for Fig. 5B, M–L–H for Fig. 5C, and M–L–H for Fig. 5D, respectively. Thus, for Fig. 5A and B, the compound jets were formed with greater viscosities than sheath, while the viscosities of PLGA solutions for Fig. 5C and D were lower than sheath.

Jet breakup time, in general, tends to increase with viscosity. Thus, the flow rates of each case were slightly altered to acquire synchronous jet breakup for each component fluid in the compound jet at different concentration combinations. For Fig. 5A, the PLGA solution had the highest viscosity which means the jet breakup time was longer than the others. Thus, breakup time was matched by increasing the core jet diameter. In the case of Fig. 5B, the relative viscosity between PLGA and lysozyme solutions was close to unity; thus, the most synchronous jet breakup resulted. For Fig. 5C and D, the relative viscosities were less than unity, that is, the viscosity of the PLGA solutions was lower than that of the core fluid. In this case, the polymer solution flow rates were increased to acquire synchronous jet breakup.

The microcapsule and core sizes were predicted analytically and compared with graphically measured values. The drop diameter was calculated by

$$d_d = \left(\frac{6Q}{\pi} t_{cap}\right)^{1/3} \tag{1}$$

where ρ and $Q$ are respectively the density and jet flow rate, $t_{cap}$ is the capillary time, which is given by $\left(\rho d_j^3 \Big/ 8\gamma\right)^{1/2}$ (27), where $d_j$ and γ are the jet diameter and interfacial tension. The jet diameter was analytically derived using the pressure balance across the interface with the Young–Dupre relation between the adjacent two fluids:

$$d_j^{-4} + \left(\frac{\pi^2\gamma}{2\rho_j Q_j^2}\right) d_j^{-1} = \frac{\pi^2}{16D^4}\left[\left(\frac{\rho_s Q_s^2}{\rho_j Q_j^2}\right) + \frac{256 Q_s \mu_s \chi}{\rho_j Q_j^2 \pi}\right] \tag{2}$$

where $D$ and $d_j$ are respectively the width of the square channel and jet diameter, χ is the distance from the square channel entrance to the position where the jet diameters are measured, and the subscripts $j$ and $s$ represent jet and sheath, respectively. The additional pressure loss was considered from the wall friction in the microchannel, i.e. Poiseuille flow, with the hydraulic diameter assumption.

Fig. 6 shows the microcapsule and core diameters acquired from the MiCE system and Eq. 1. In Fig. 6, $Q_{jet}$ is the flow rate of the compound jet. The microcapsule diameters observed in the microchannel ranged from about 50–100 μm and were well predicted with Eq. 1, while the core diameters were slightly under-predicted. Both microcapsule and core diameters increased with compound jet flow rate. Also, the effect of viscosity variation is somewhat indistinctive, while responses to slight flow rate changes are clearly shown. The analysis shows that viscosity exerts a greater effect on the core diameter than the microcapsule diameter. For lower PLGA solution viscosities, the core diameter increases with jet flow rate to a greater extent. This is because the viscous stress exerted on the core jet becomes greater at higher concentrations of PLGA solution, which prevents widening of the core jet under larger flow rates.

**Fig. 10.** SEM images of microcapsules produced using the MiCE process. **A** and **B** 5%, **C** and **D** 3.5%, **E** and **F** 2.5%, and **G** and **H** 1.5% PLGA in ethyl acetate. Aqueous core solution: 3% lysozyme in distilled water. Sheath and collection bath: distilled water. **B**, **D**, **F**, and **H** are 5× magnifications of the areas outlined in **A**, **C**, **E**, and **G**, respectively. For **A**, **C**, **E**, and **G**, *scale bars*=10 μm. For **B**, **D**, **F**, and **H**, *scale bars*=1 μm. ▶

## Microcapsule Collection

Experiments were performed with 5, 3.5, 2.5, and 1.5% PLGA in ethyl acetate solutions and a 3% aqueous lysozyme solution. Four different batches were run through the system. Qualitative observations on size and morphology of the collected microcapsules were made using bright field and fluorescent microscope imaging (Fig. 7 and 8). Additionally, SEM imaging (Fig. 10) was used to determine microcapsule morphology, polymer membrane integrity, and freeze-drying effects. From Fig. 7 and 8, large size distributions and various morphologies can be observed. Both thin- and thick-walled single-core microcapsules were generated, in addition to smaller multi-core ones. These results are quite different from the 50–100 μm microcapsule and single-core morphologies observed within the microchannel. The main cause of this large discrepancy in microcapulse size and morphology is the secondary breakup of microcapsules due to Kelvin–Helmholtz instabilities, which are encountered when a jet is issued into a stagnant medium such as the collection bath (Fig. 9). Since the microchannel tip was submerged below the surface of a stagnant aqueous collection bath, and the stream

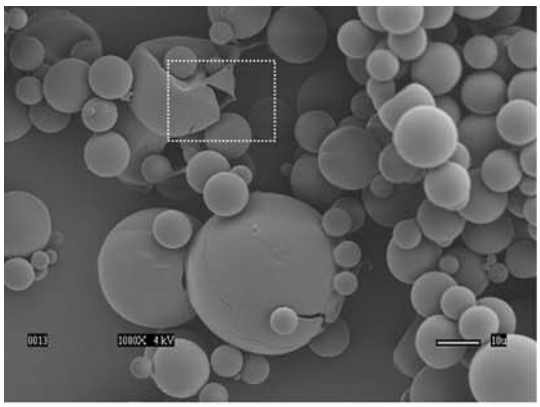
0011
1000X 4kV
10u

(A)

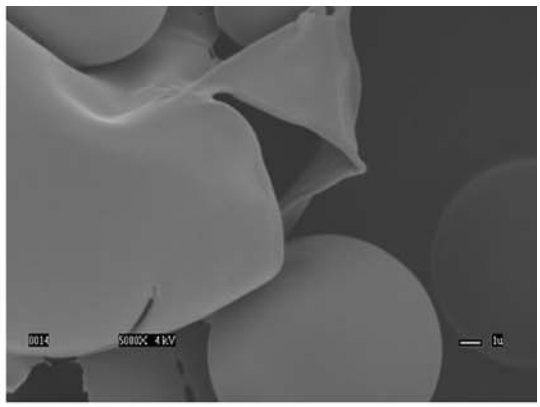
0014
5000X 4kV
1u

(B)

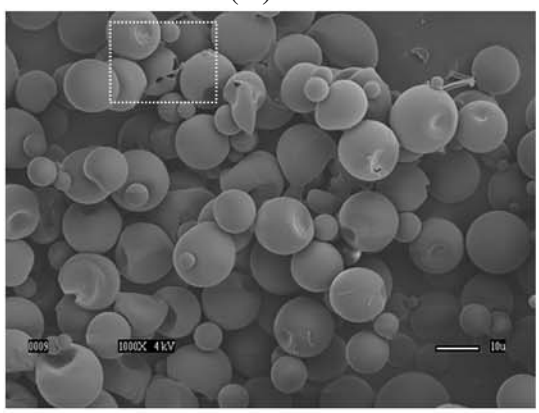
0009
1000X 4kV
10u

(C)

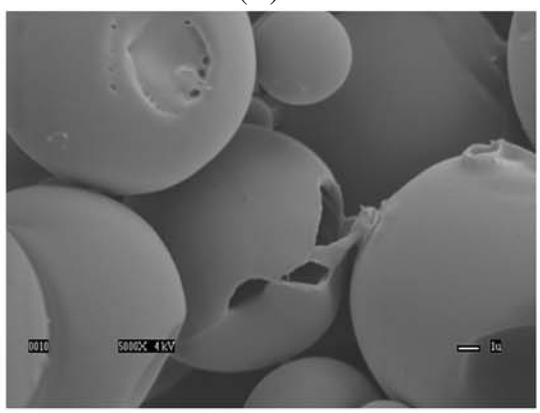
0010
5000X 4kV
1u

(D)

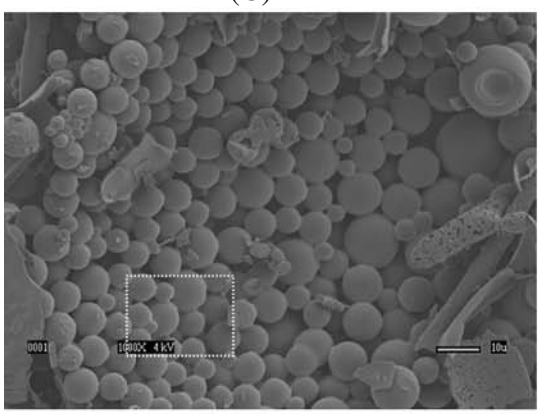
0001
1000X 4kV
10u

(E)

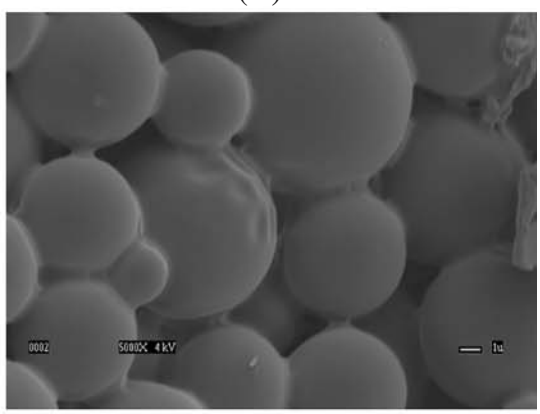
0002
5000X 4kV
1u

(F)

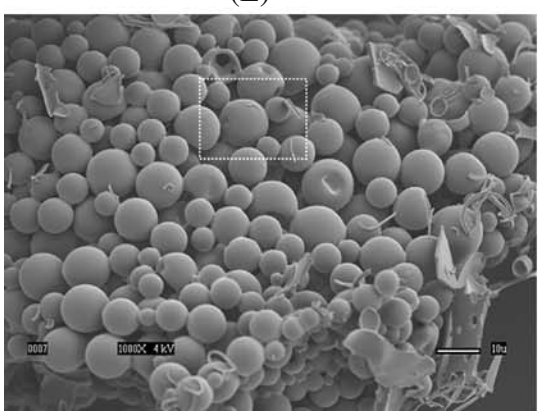
0007
1000X 4kV
10u

(G)

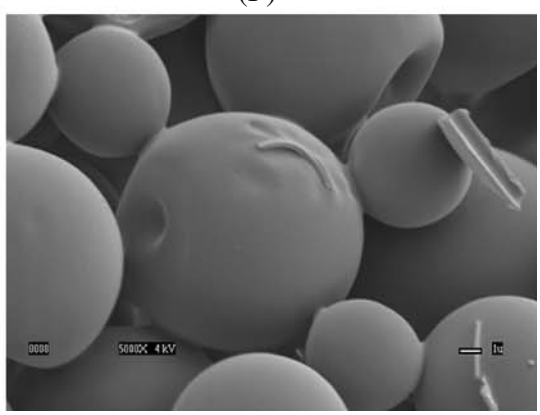
0008
5000X 4kV
1u

(H)

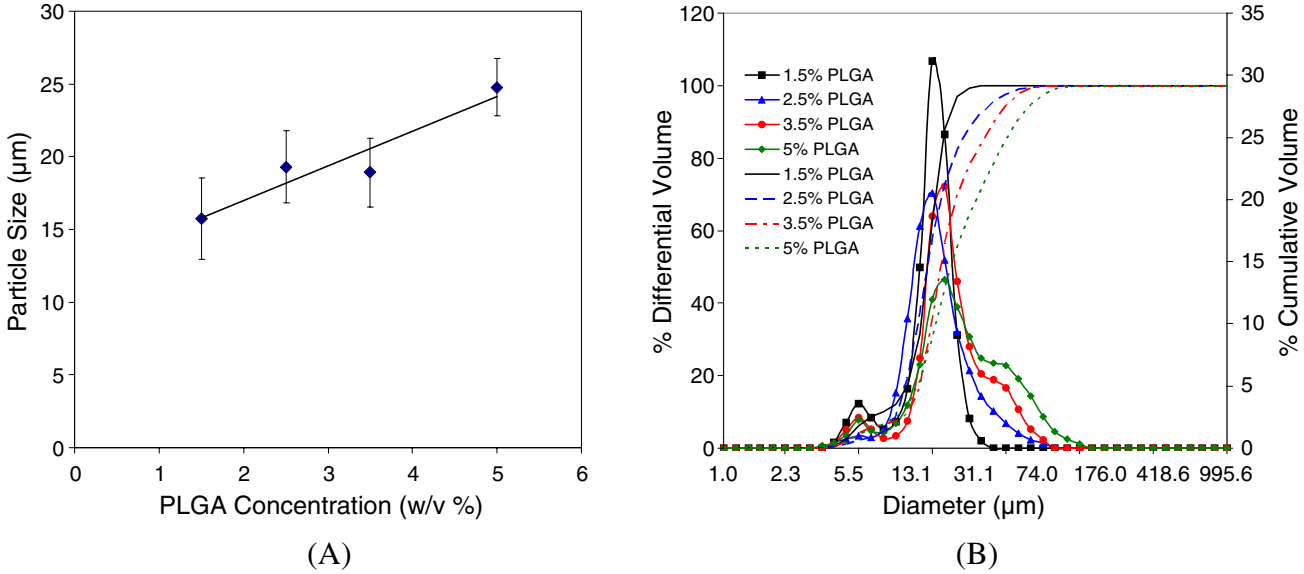


**Fig. 11.** **A** Relationship between PLGA concentration and the mean microcapsule sizes after secondary breakup. **B** Size distributions of the microcapsules after secondary breakup.

eluting from the microchannel has a relatively high velocity of approximately 3.5 m/s, nascent microcapsules are exposed to large shear forces, which form an unstable cylindrical shear layer with ring vortices (28). Fig. 9 shows how microcapsules initially exiting the microchannel serially march into the collection bath (Fig. 9A) and eventually undergo secondary breakup (Fig. 9C).

The secondary breakup may be the reason for rather low encapsulation efficiency. The encapsulation efficiency was a function of the flow rates of protein and PLGA solutions, and it ranged from 5% to slightly more than 30%. The poor encapsulation efficiency led to a low protein loading efficiency (i.e., weight percent) of less than 20%. The secondary breakup of microcapsules is more pronounced when the microcapsules are large and polymer membranes are thin since these thin-walled microcapsules have less structural stability. In addition, the secondary breakup depends on the competition between external and internal forces due to surface tension and viscosity, such that surface tension is a disruptive force and viscosity is a stabilizing force (29). Since the flow rates of the carrier stream (sheath) remained at about 13 mL/min from batch to batch, the changing viscosity is the factor most likely causing the microcapsule size change. This viscosity effect on the secondary breakup is shown in the bright field and SEM images in Fig. 7 and Fig. 10, respectively. From these images, we can see that the microcapsule diameter gradually decreases as the PLGA concentration decreases. Also, as the microcapsule sizes become progressively smaller, the polymer membrane becomes progressively thicker, which is best noticed from the SEM images. In Fig. 10B, the polymer membranes of two larger microcapsules, about 40 μm in diameter, are quite thin, while the membrane of a smaller microcapsule in Fig. 10D, about 15 μm in diameter, is considerably thicker. A likely cause for this result is the secondary breakup. This breakup causes the polymer shell to transiently rupture, allowing some of the drug core contents to be released. As a result, the relative amount of PLGA solution to drug solution is greater, leading to a thicker-walled microcapsule. Also, the surface of the microcapsules in these SEM images is very smooth, indicating the absence of pores in the membrane. This implies that drug release will occur via biodegradation (i.e. hydrolysis) of the PLGA.

### Particle Size Analysis

After the microcapsules were freeze-dried, they seemed to be attached to one another in a web-like fashion, and this webbing appeared to increase as the PLGA solute concentration decreased. These attachments can be noticed in the SEM images (Fig. 10) and were a result of no microcapsule cleaning step, prior to lyophilization. Because microcapsule washing, consisting of a fresh water rinse, centrifugation, and discarding the supernatant, was never carried out for these batches, unencapsulated protein and any remaining ethyl acetate were left in the collection bath liquid surrounding the microcapsules. Therefore, the microcapsule attachments may have been comprised of lysozyme and/or ethyl acetate. The presence of ethyl acetate in the surrounding bath can cause the PLGA membranes to remain partially unsolidified. After freeze-drying, the material comprising the attachments was tested using the bicinchoninic acid protein assay. It was found that a great deal of lysozyme comprised them, and the protein concentration did decrease for larger PLGA concentrations. This result is expected since less secondary breakup takes place in the microchannel for more highly-concentrated PLGA solutions, causing the encapsulation efficiency to be higher.

A correlation was found between the PLGA solution viscosity and microcapsule mean diameter (Fig. 11A). As we expected, when the viscosity of the polymer solution was increased, the mean microcapsule diameter increased. Also, an increased viscosity brought about a wider size distribution (Fig. 11B) for more viscous polymer solutions. The bimodal characteristics displayed in the size distributions were present for every PLGA concentration, where the smaller peak existed for diameters around 5.5 μm. This peak may have

resulted from ruptured polymer membranes in the collection bath. Since higher viscous forces can stabilize larger microcapsules and prevent excessive rupturing, we can expect that a higher PLGA concentration yields a wider size distribution. Thus, our predictions from the bright field and SEM imaging were confirmed by these results.

## CONCLUSIONS

A new MiCE microencapsulation process based on the natural jet segmentation employed in flow cytometry has been explored. The microencapsulation proceeds via hydrodynamic focusing of the component drug and PLGA solutions into a narrowed jet, which is then segmented due to Rayleigh-type instabilities within a quartz microchannel. When the polymer solution solvent diffuses into a surrounding aqueous sheath, PLGA precipitation can take place and leads to hardening of the nascent microcapsules. The entire microencapsulation process can be viewed in real-time, a feature that brings about real-time fine-tuning of those mechanical parameters that result in desired microcapsule attributes, including size, core size, membrane thickness, and morphology. The primary determinants of these microcapsule attributes are the working fluid flow rates since their precise modification can result in proper jet breakup dynamics. Using the MiCE process, we produced microcapsules with small mean diameters ranging from 15–25 μm. Optimization of this system however, requires prevention of the secondary breakup that occurs within the microchannel through formulation and/or mechanical modifications. It was found that a more highly-concentrated PLGA solution provided enough stabilizing viscous forces to decrease secondary breakup in the collection bath. Further prevention of this breakup is expected to greatly increase the encapsulation efficiency and decrease the microcapsule size distribution, which can lead to more predictable release kinetics. Following further optimization, the MiCE process has the potential to become an effective microencapsulation method.

## ACKNOWLEDGEMENTS

This research project was funded in part by the NSF/Integrative Graduate Education and Research Traineeship Program on Therapeutic and Diagnostic Devices (grant DGE-99-72770) and the National Institutes of Health (grants GM67044 and EB003584).

## REFERENCES

1. S. P. Schwendeman, *et al*. Stability of proteins and their delivery from biodegradable polymer microspheres. In S. Cohen and H. Bernstein (eds.), *Microparticulate Systems for the Delivery of Proteins and Vaccines*, Marcel Dekker, New York, 1996, pp. 1–49.
2. Y. Yeo, N. Baek, and K. Park. Microencapsulation methods for delivery of protein drugs. *Biotechnol. Bioprocess Eng.* **6**(4):213–230 (2001).
3. G. Zhu, S. R. Mallery, and S. P. Schwendeman. Stabilization of proteins encapsulated in injectable poly(lactide-co-glycolide). *Nat. Biotechnol.* **18**:52–57 (2000).
4. M. E. Keegan *et al*. *In vitro* evaluation of biodegradable microspheres with surface-bound ligands. *J. Control. Release* **110**(3):574–580 (2006).
5. J.-P. Benoit *et al*. Biodegradable microspheres: advances in production technology. In S. Benita (ed.), *Microencapsulation: Methods and Industrial Applications*, Marcel Dekker, New York, 1996, pp. 35–72.
6. P. Couvreur *et al*. Multiple emulsion technology for the design of microspheres containing peptides and oligopeptides. *Adv. Drug Deliv. Rev.* **28**(1):85–96 (1997).
7. J. H. Park et al. Reservoir-type microcapsules prepared by the solvent exchange method: effect of formulation parameters on microencapsulation of lysozyme. *Mol. Pharm.* **3**(2):135–143 (2006).
8. F. Gu, R. Neufeld, and B. Amsden. Sustained release of bioactive therapeutic proteins from a biodegradable elastomeric device. *J. Control. Release* **117**(1):80–89 (2007).
9. J. D. Andrade and V. Hlady. Protein adsorption and materials biocompatibility: a tutorial review and suggested hypotheses. *Adv. Polym. Sci.* **79**:1–63 (1985).
10. H. Sah and Y. Bahl. Effects of aqueous phase composition upon protein destabilization at water/organic solvent interface. *J. Control. Release* **106**(1–2):51–61 (2005).
11. L. Rayleigh. On the capillary phenomena of jets. *Proc. R. Soc. Lond.* **29**:71–97 (1879).
12. L. Rayleigh. On the instability of jets. *Proc. Lond. Math. Soc.* **10**:4–13 (1879).
13. G. Durack. Cell-sorting technology. In G. Durack and J.P. Robinson (eds.), *Emerging Tools for Single-Cell Analysis: Advances in Optical Measurement Technologies*, Wiley-Liss, New York, 2000, pp. 1–19.
14. H. M. Shapiro. *Practical Flow Cytometry. 4th ed.*, John Wiley & Sons, Hoboken, New Jersey, 2003.
15. C. H. Hertz and B. Hermanrud. A liquid compound jet. *J. Fluid Mech.* **131**(Jun):271–287 (1983).
16. C. Berkland *et al*. Three-month zero-order piroxicam release from monodispersed double-walled microspheres of controlled shell thickness. *J. Biomed. Mater. Res.* **70**(4):576–584 (2004).
17. C. Berkland, K.K. Kim, and D.W. Pack. Precision microcapsules with controlled diameter and shell thickness. In *29th International Symposium on Controlled Release of Bioactive Materials*, Seoul, Korea, 2002.
18. C. Berkland *et al.* Uniform double-walled polymer microspheres of controllable shell thickness. *J. Control. Release* **96**:101–111 (2004).
19. I. G. Loscertales *et al*. Micro/nano encapsulation via electrified coaxial liquid jets. *Science* **295**:1695–1698 (2002).
20. A. M. Gañán-Calvo and J. M Gordillo. Perfectly monodisperse microbubbling by capillary flow focusing. *Phys. Rev. Lett.* **87**(27):1–4 (2001).
21. A.S. Utada *et al*. Monodisperse double emulsions generated from a microcapillary device. *Science* **308**:537–541 (2005).
22. W. C. Elmore and M. A. Heald. *Physics of waves*, McGraw-Hill, New York, 1969.
23. L. E. Johns and R. Narayanan. *Interfacial instability*, Springer, New York, 2002.
24. Y. Yeo, O. A. Basaran, and K. Park. A new process for making reservoir-type microcapsules using ink-jet technology and interfacial phase separation. *J. Control Release* **93**:161–173 (2003).
25. D. R. Lide. *CRC Handbook of Chemistry and Physics, 85th ed*, CRC Press, Boca Raton, (2004).
26. N. V. R. Rao and M. H. I. Baird. A simple technique for the measurement of surface and interfacial tension. *J. Phys. E.* **16**(12):1164–1166 (1983).
27. Eggers J. Nonlinear dynamics and breakup of free-surface flows. *Rev. Mod. Phys.* **69**(3):865–929 (1997).
28. A. M. Gañán-Calvo and A. Barrero. A novel pneumatic technique to generate steady capillary microjets. *J. Aerosol Sci.* **30**(1):117–125 (1999).
29. H. Liu. *Science and Engineering of Droplets—Fundamentals and Applications*. William Andrew Publishing/Noyes, Norwich, New York, 2000.